International Journal of Fluid Power 10 (2009) No. 3 pp. 17-27

MODEL DEVELOPMENT AND EXPERIMENTAL ANALYSIS OF A VIRTUALLY VARIABLE DISPLACEMENT PUMP SYSTEM

John Lumkes Jr., Mark A. Batdorff and John R. Mahrenholz

Purdue University – Agricultural & Biological Engineering Dept. 225 South University Street, West Lafayette, IN 47907 USA
lumkes@purdue.edu, mbatdorf@purdue.edu, jmahrenh@purdue.edu

Abstract

This work presents the modelling and testing of a Virtually Variable Displacement Pump (VVDP). The system used a high speed on/off valve to modulate flow from a fixed displacement pump, directing the flow either to the tank or high pressure supply line of the hydraulic system. A lumped parameter model of the system was developed using sub-models to describe the dynamics of each component in the system. A test setup using currently available components was built to validate the overall system model and study the effects of switching frequency on system efficiency. Once verified, the model was used to simulate and further study the effects of changing the compressible fluid volume and line lengths. Simulation results show that reducing the line lengths and compressible volume improves the average VVDP system efficiency by 14 % over a range of switching frequencies and duty cycles while holding other system parameters constant.

Keywords: virtual variable displacement pump, lumped parameter model, verification, optimization

1 Introduction

Traditional fluid power systems using resistive control of hydraulic actuators are inefficient under most operating conditions since excess hydraulic power is dissipated as heat by metering the flow through control valves. By incorporating variable displacement pumps, recent hydraulic systems utilize pressure-compensated load sensing systems to help minimize these metering losses and improve system efficiency. These systems work well when all the actuators require nearly the same pressure to operate but they experience reduced efficiency when one actuator requires a pressure that is much higher than the remaining actuators. In addition, the efficiency of these systems is reduced when the variable displacement pump operates at low displacement settings. To further reduce metering losses researchers have studied the use of using an individual variable displacement pump for each actuator (Grabbel and Ivantysynova, 2005; Heybroek et al. 2006; Williamson et al., 2008), using independently controlled metering orifices to reduce the metering losses when valves are used (Shenouda and Book, 2008; Liu and Yao, 2002), or recovering energy using a secondary pressure rail (Andruch and Lumkes, 2008).

This manuscript was received on 30 March 2008 and was accepted after revision for publication on 25 August 2009

One disadvantage of these systems is the requirement for a variable displacement pump (and motor in some cases), which increases the cost. In many applications, such as excavators and wheel loaders, the increased costs can be justified through the improved efficiency which leads to financial savings through reduced fuel consumption. For applications where this might not be true, such as charge pump systems (due to the lower power levels), log splitters, and light duty occasional use off-road machines, some of the advantages of using a variable displacement pump can be achieved using a fixed displacement, low cost pump (gear pump or similar) and a high-speed on/off valve to switch the flow either to the tank or high pressure line of the hydraulic system. This option has come to be known as a Virtually Variable Displacement Pump (VVDP). The valve is operated discretely in one of two states. In the system state, pressure and flow are directed from the pump (Port A) to the system (Port B). When the valve is shifted to the tank state, flow from the pump (Port A) is directed to the tank (Port C). By varying the proportion of time, also known as duty cycle, that the pump is connected to system or tank, the net system flow rate can be altered (Batdorff and Lumkes, 2006; Li et al., 2005; Mahrenholz, 2009; Neiling et al., 2005; Tu et al., 2008).

When the on/off valve is fully open the system experiences reduced metering losses compared with traditional resistance based control valves. Although a variable displacement pump is not needed, in a VVDP system the efficiency is highly dependent on system parameters such as valve switching time, valve flow area, compressibility, and overall switching frequency. A VVDP system will never exceed the overall efficiency of the fixed displacement pump; it only reduces the losses due to metering in a traditional system. Besides the challenging valve requirements, more components are needed relative to a variable displacement pump and the effects of switching the system flow can induce noise into the system.

In a VVDP system there is a design tradeoff between switching frequency and system efficiency. Lower switching frequencies reduce the metering losses that occur during valve transition times but increases the pressure ripple, assuming other system components, i.e. accumulator size remains the same (Batdorff and Lumkes, 2006). The compressible volume between the pump and switching valve is also important. Each time the valve switches and connects the pump flow to the system, the fluid must increase in pressure up to the system pressure before positive work is done on the system. This compressible work is not recovered during decompression when the valve is switched again to connect the pump with the tank line.

The work presented in this paper studies these effects and focuses on VVDP system development, modeling, testing, and optimization. Using a prototype valve the system shown in Fig. 1 was built and tested in the laboratory to verify the overall structure and parameter values used in the model. This model was then used to study the effects of changing components and parameters in the system to maximize the VVDP efficiency.

2 Physical System Setup and Design

The configuration examined during this research used an open-center three-port two-position valve with a backflow prevention check valve. The check valve prevents fluid from the system from flowing back to tank while the switching valve is in the open-center portion of its transition. The addition of this check valve improves the efficiency but requires an additional component. It is possible to remove the check valve by incorporating a two-position switching valve with a closed-center during transition (over-lapped), thus keeping the high and low pressure ports isolated during transition. The switching valve available for this project was open-center and required the check valve to minimize energy losses during switches. An accumulator is used to smooth the flow ripple created by the valve switching. A diagram of this system is shown in Fig. 1.

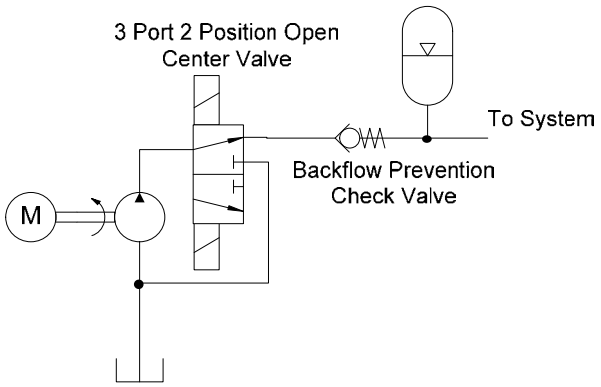

Fig 1: *Open-Center 3/2 VVDP System w/ Backflow Prevention Check Valve*

2.1 On/Off Valve

The on/off valve used for this research was a three-port, two-position, open-center valve (Mahrenholz, 2009). A cutaway of this valve is shown in Fig. 2. Steel parts of the design include the coil cups and force ring. All other parts are aluminum.

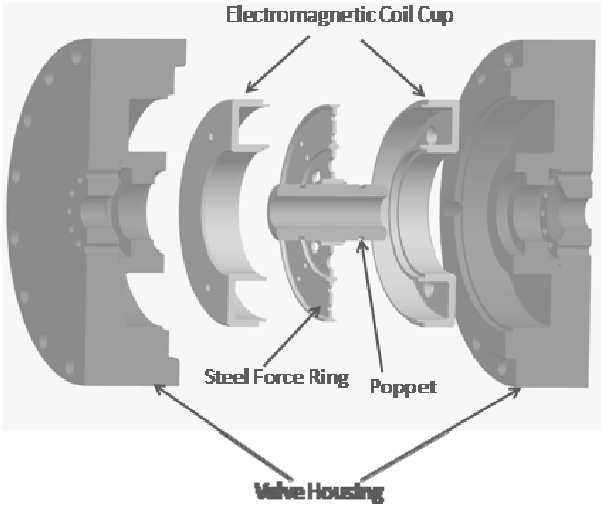

Fig. 2: *High Speed On/Off Valve Cutaway*

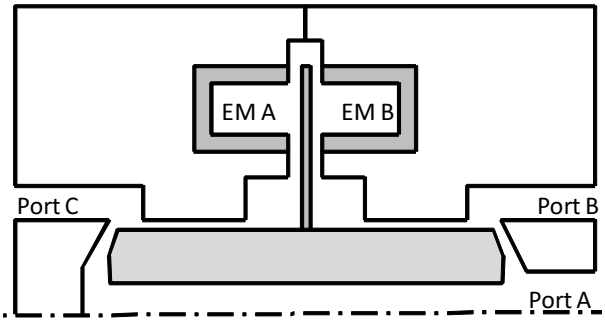

Fig 3: *High Speed On/Off Valve Functional Drawing*

The material, electromagnetic, and fluid features of the valve used in this study are illustrated in Fig. 3. Copper windings, shown as EM A and EM B, are placed in each of the two steel cups. By activating a winding, an electromagnetic flux path is formed running through the steel cup and the center force ring. This flux path draws the steel center force ring towards the steel cup, thus shifting the poppet towards that side.

For instance if coil EM A was activated the poppet would be pulled left. This movement causes port A to be connected to port B, while port C is then blocked off. Similarly, by activating EM B the poppet shifts rightward connecting ports A and C while blocking port B. During transition the valve is open-center and all three ports are connected.

2.2 Check Valve

The check valve used in this system is from a disk style discharge check valve used in John Deere 3000 series radial piston pump. This check valve, shown in Fig. 4, consists of five major components. The primary component of this valve is the steel disk. This part replaces the ball used in most check valves. The disk has a higher pressure area to mass ratio than a normal ball style check valve and therefore its closing and opening speeds are also higher. The disk, directed by a sheet metal guide, seats flat against a piece of hardened steel. A spring is used to hold the check valve closed under no flow conditions. Finally, a plug is used to contain the entire check valve assembly.

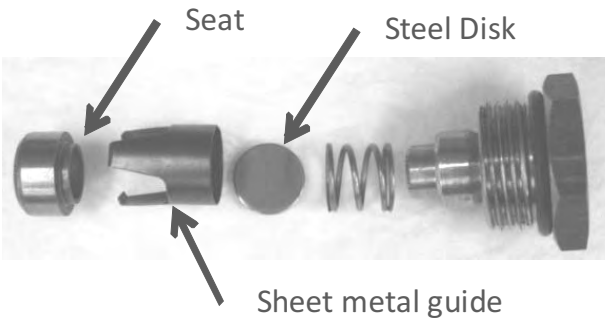

Fig. 4: *High Speed Check Valve*

2.3 Prime Mover / Pump

The prime mover for this system was a 5.6 kW electric motor with a variable frequency drive. This motor is capable of 0 to 3600 rpm output speeds and a maximum torque of 15 Nm. While normally a variable frequency drive would not be required for a VVDP system, one was used in this case to verify performance over a range of input speeds and flow rates. The motor was used to drive a 9.8 cc Parker Hannifin F11 bent axis fixed displacement pump. A 2:1 reduction was used between the electric motor and pump. This reduces torque requirements on the electric motor when the pump is operated at high pressures.

2.4 Accumulator and Load Simulator

The accumulator used in this system has a volume of 0.94L, a pre-charge pressure of 35 bar, and a piston mass of 0.12 kg. A piston type accumulator was used because of availability. Bladder type accumulators, with less moving inertia, respond more quickly to the pressure changes.

The load simulator for the VVDP system consists of three valves. The safety relief valve is used to limit maximum system pressure and protect the electric motor from stalling. A relief pressure of 175 bar ensures that the maximum available motor torque is never exceeded. The constant pressure load valve is adjusted to maintain desired system pressure. Finally a solenoid operated load release valve is used to release system pressure during start-up and shut down conditions. The load system and accumulator are shown in Fig. 5.

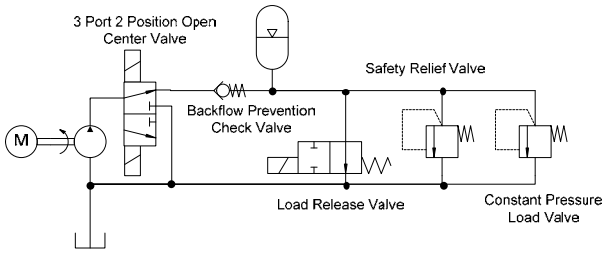

Fig. 5: *VVDP System with Load Simulator*

2.5 Valve Driving Hardware and Control States

Figure 6 shows the circuit used to control one coil within the valve. This circuit consists of an H-bridge using two MOSFETs with integrated Zener diodes and two independent diodes. The MOSFETs are driven using an IRS2117 single channel MOSFET driver (not shown) that maintains the gate voltage 10 V above the floating source voltage.

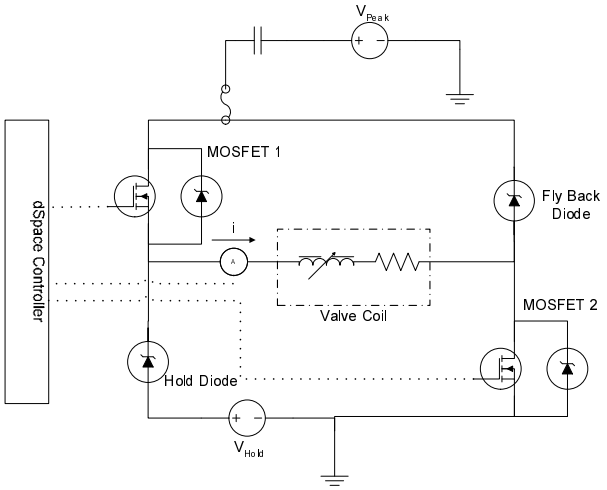

Fig. 6: *Driving Circuit Schematic*

For this circuit, three states are used. In the hold state, MOSFET 2 is activated. Current then flows from the hold voltage source through the hold diode and the coil left to right and finally to ground. In the peak state, MOSFETs 1 and 2 are activated. Current then flows from the peak voltage source through the coil left to right and finally to ground. In the off state, both MOSFETs are deactivated. Once the MOSFETs are deactivated, the inductance of the coil causes freewheeling current to flow through the hold diode and be pushed through the fly back diode. Because this action causes a voltage rise, a decay voltage equal to the voltage rise (V_{Peak} - V_{Hold}) is imposed upon the coil. This voltage rise forces the coil current to rapidly decay.

3 Simulation

A model was developed to simulate the effect of changing system parameters and the resulting impact on system efficiency. The model was developed using Matlab Simulink® and Matlab Simscape® as the core modeling

and solving utilities. Simscape is a power based modeling package that allows for in line modeling of flow and effort in the hydraulic, electrical, thermal, and mechanical domains. Detailed models of the pump, on/off valve, and constant pressure load valve were developed in earlier research (Mahrenholz, 2009). The following sections will present a brief overview of these models.

3.1 Prime Mover/Pump Model

The pump and prime mover model consists of an ideal flow source coupled with a compressible volume. This flow source generates a net system flow using the pressure build up relationship within the compressible volume. The flow due to compressibility is defined as:

$$V_{comp} = V_{line} - \frac{V_{line}}{\beta} p_{line} \tag{1}$$

and

$$Q_{comp} = \frac{dV_{comp}}{dt} \tag{2}$$

where β is defined as the isothermal bulk modulus.

3.2 On/Off Valve Model

Figure 7 shows the general layout of the on/off valve model. The model itself is composed of three different domains: electromagnetic, fluidic, and mechanical.

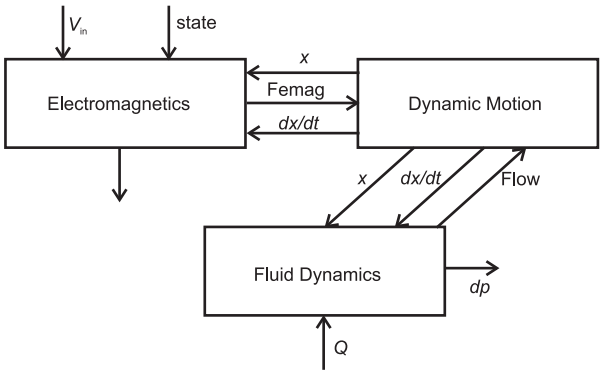

Fig. 7: *On/Off Valve Model Overview*

The electromagnetic domain has inputs of driving voltage (V_{in}), control state, poppet position (x), and poppet velocity (dx/dt). Using lumped parameter equations that consider non-linear effects such as inductance, fringing, and eddy currents, this model outputs the electromagnetic force (F_{emag}) and coil current (i).

The fluidic domain has inputs of flow rate (Q), valve position and valve velocity. A lumped parameter model of gap and poppet flow forces develops both steady state and dynamic forces from the fluid interaction with the poppet. These forces are lumped together (F_{flow}) and applied to the mechanical domain.

The mechanical domain uses force from the electromagnetic and fluidic domains in addition to wall forces (F_{wall}) to determine net force on the poppet. Using this net force and poppet mass, this domain model calculates acceleration and integrates to find poppet velocity and position which is then fed back to the electromagnetic and fluidic domains. In this manner, all three domains are coupled together as shown in Fig. 8. This earlier work was experimentally verified and allows the valve model to predict the valve transition profile under a variety of driving voltages, flows, and pressures (Mahrenholz and Lumkes, 2009). The coupled valve model was then used to determine valve transition profiles for the simulation described in this paper. The fully coupled valve model was originally coupled with the VVDP simulation, leading to long solution times and problems with convergence when the check valve, line, fluid, and accumulator models were added. Subsequently, the valve model was simulated first and the valve characteristics (transition profile) applied to the VVDP model. The valve lag time and transition time were typically 2 ms and 1 ms, respectively, and relatively insensitive to flow and pressure variations.

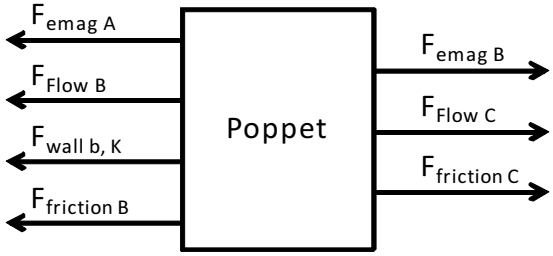

Fig. 8: *Forces acting on poppet in On/Off Valve*

3.3 Constant Pressure Load Valve Models

Both the safety relief and constant pressure load valve are modeled using an ideal relationship between pressure and area. This area is then applied to a variable orifice block in Simscape to produce a flow path to the reservoir. The relationship between system pressure and orifice area is defined as:

$$A_{rel} = \begin{cases} (p_A - p_T - p_{set})k_{rel} & for \;\; p_A - p_T \geq p_{set} \\ 0 & for \;\; p_A - p_T < p_{set} \end{cases} \tag{3}$$

where p_A is the pressure at the inlet of the valve and p_{set} is the desired load pressure for the system.

3.4 Check Valve Model

The dynamics of the check valve can have a large impact on the efficiency of VVDP systems. A pressure affected mass, spring, and hard stop are used to model the check valve. This model assumes a linear spring and no drag on the disk of the check valve.

The force due to pressure on the check valve is equal to the pressure affected area times the pressure differential across the valve.

$$F_{cv\,press} = A_{cv}\left(\Delta p_{cv}\right) \tag{4}$$

The spring force on the check valve is modeled using a linear spring coefficient and the valve position.

$$F_{cv\,spring} = k_{cv} x_{cv} \tag{5}$$

The hard stop is modeled as a stiff spring and dampener dependent on the intrusion into the wall. This intrusion is defined as:

$$x_{cv\,wall} = \begin{cases} x_{cv} - x_{cv\,max} & for \; x_{cv} \geq x_{cv\,max} \\ 0 & for \; 0 < x < x_{cv\,max} \\ -x_{cv} & for \; x_{cv} \leq 0 \end{cases} \tag{6}$$

The spring force is then simply the intrusion multiplied by the wall spring coefficient.

$$F_{\text{cv wall K}} = -k_{wall}\, x_{\text{cv wall}} \tag{7}$$

The damping force is assumed to be proportional to velocity while in contact with the wall.

$$F_{\text{cv wall b}} = \begin{cases} -\dfrac{dx_{\text{cv}}}{dt} b_{\text{wall}} & for\ x_{\text{cv}} \geq x_{\text{cv max}}\ or\ x \leq 0 \\ 0 & else \end{cases} \tag{8}$$

The net force on the check valve is then the sum of these components. This force is divided by the mass of the check valve (m_{cv}) to determine acceleration which is integrated to find velocity and integrated again to determine position.

3.5 Accumulator Model

The accumulator is modeled as two variable volume chambers where the volumes of the chambers are separated by a piston with mass m. The force balance on the accumulator is shown in Eq. 9.

$$m\ddot{x} = \sum Forces = F_{\text{oil side}} - F_{\text{gas side}} - F_{\text{friction}} \tag{9}$$

The force acting the oil side of the piston is

$$F_{\text{oil side}} = A_{\text{piston}}\ p_{\text{system}} \tag{10}$$

where A_{piston} is the area of the accumulator piston and p_{system} is the pressure of system between the check valve and load valve. The force acting on the gas side of the piston is

$$F_{\text{gas side}} = A_{\text{piston}}\ p_0 \left(\frac{V_{\text{o}}}{V_0 - A_{\text{piston}}\, x} \right)^n \tag{11}$$

where p_{o} is the accumulator charge pressure, V_{o} is the accumulator initial volume, x is the position of the piston (x=0 when there is $p_{\text{system}} = p_{\text{o}}$), and n=1.4 for adiabatic operation. The friction force acting on the piston is

$$F_{\text{friction}} = b\,\dot{x} + c\frac{\dot{x}}{|\dot{x}|} \tag{12}$$

where b is the viscous damping coefficient and c is the coulomb friction force.

3.6 Line Models

The line model used in this work consists of two elements – inertia and resistance. The compressible volumes were lumped and combined with other oil volumes at both ends of the hose. The pressure drop due to inertia of the line segment is modeled as:

$$p_{\text{iner}} = \rho \frac{L}{A} \frac{dQ_{\text{line}}}{dt} \tag{13}$$

where L and A are the length and area of the hose respectively.

The total hose resistive pressure drop is calculated as:

$$p_{\text{res}} = f \frac{L}{d} \frac{\rho}{2A^2} Q_{\text{line}} \left| Q_{\text{line}} \right| \tag{14}$$

where f is the friction factor (Moody diagram) describing the hose and d is the diameter of the hose.

4 Performance Results

4.1 Test Setup

Table 1 provides the physical system parameters for the laboratory VVDP setup.

Table 1: Test Setup Parameters

Symbol	Parameter	Value
--	Switching Frequencies	Varies
$\%\text{Duty}_{\text{cycle}}$	% Duty Cycle	Varies
V_{hold}	Hold Voltage	14 V
V_{peak}	Peak Voltage	60 V
q_{inlet}	Valve Inlet Flow	8.7 L/min
p_{system}	System Pressure Setting	58 bar
V_{line}	Compressible Volume	70 cc
L	Line Length	122 mm
d	Line Diameter	9.5 mm
m_{cv}	Check Valve Mass	0.00279 kg
A_{cv}	Check Valve Area	86.4 mm^2
$x_{\text{cv max}}$	Check Valve Minimum Position	3.6 mm
m	Accumulator Piston Mass	0.12 kg
A_{piston}	Accumulator Piston rea	2055 mm^2
b	Viscous Damping Coefficient	700 N sec/m
c	Coulomb Friction Force	18 N
V_0	Accumulator Initial Volume	0.94 L
p_0	Accumulator Precharge	35 bar
ρ	Density of oil	850 kg/m^3

Sensors were added to the physical system test setup as shown in Fig. 9. Pressure sensors were placed on the inlet and system sides of the valve. A turbine flow meter was used to measure inlet flow rate, while an orifice style flow meter was used to capture system flow ripple. All three pressure transducers were WIKA 892.23.510 with a response time ≤ 1 ms. The flow meter was a Flow Technology FT-08NEU2 with a typical response time of 3-4 ms.

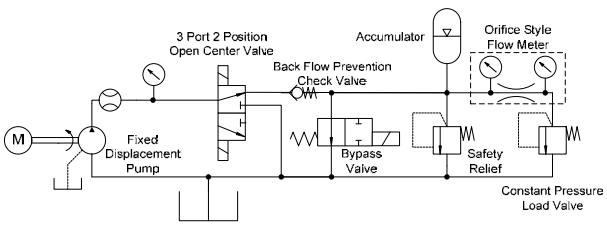

Fig. 9: *VVDP Test Setup with Sensors*

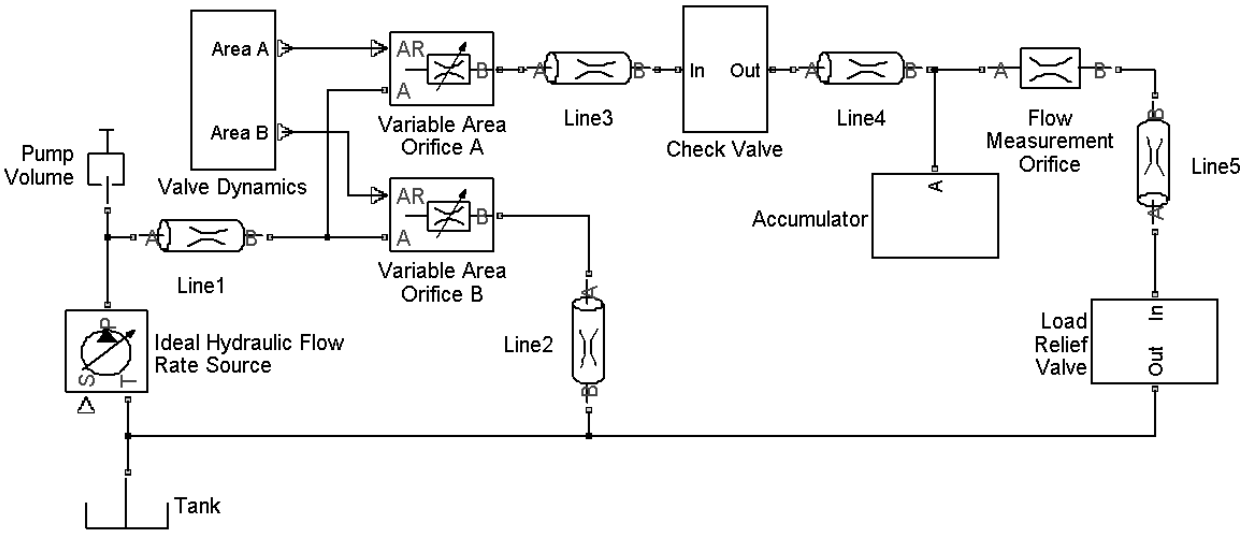

Fig. 10: *VVDP Simulink/Simscape Simplified Model*

The MATLAB-Simulink/Simscape model used for the simulation is shown in Fig. 10. The line models included resistive, inertial, and capacitive effects. The two-position three-way valve was modeled using two variable area orifices. During valve switching both orifices are partially open representing the open-center design of the valve.

4.2 Effect of Duty Cycle

The plots in Fig. 11 to 14 show the simulated and measured pressures at the inlet and system side of the valve. These tests were all performed at a switching frequency of 20 Hz with three different duty cycles.

Figure 11 and 12 show simulated and measured pressures at a 50 % duty cycle. In Fig. 11 the model captures the pressure rise accurately during each switch. However, oscillation during the high pressure portion is significantly larger in the model than in the actual data. This can be attributed to several factors. First, it is difficult to capture the effective bulk modulus due to entrapped air and the compliance added by the various hydraulic fittings and hoses connecting the components together. Second, the pressure transducers will attenuate, to some extent, the measured signal. Third, the pump pressure ripple (dependent on the type of pump chosen) is not included in the model. Fourth, the lumped parameter line model does not capture the pressure wave propogation through the line. Fifth, the system is modeled using an ideal relief valve. This results in the dynamics of these two systems having higher natural frequencies, which leads to higher frequencies in the simulated pressure profile. The spike in the low pressure portion of the valve inlet pressure models is due to fluid inertia of the return line. The model captures the amplitude of these spikes very well, with only minor errors in the frequency.

The plot in Fig. 12 shows the system pressure profile (pressure after the check valve). Although the piston mass (measured from the physical accumulator) is included in the accumulator model, the measured pressure flucuations at the beginning and end of each switch that are still not captured in the simulation. These differences in the pressure traces have negligible effects on the efficiency calculations and subsequent comparisons.

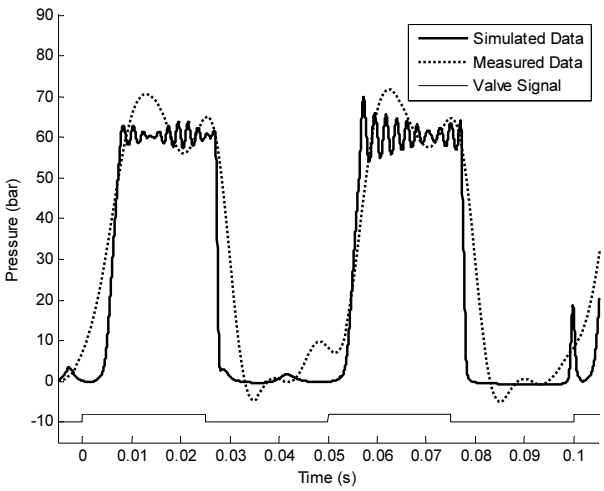

Fig. 11: *Valve Inlet Pressure @ 50 % duty cycle, 20 Hz*

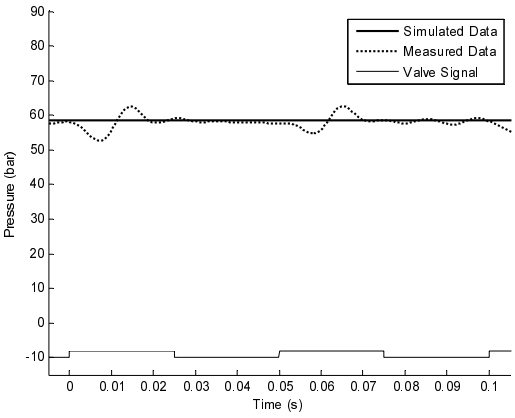

Fig. 12: *System Pressure @ 50 % duty cycle, 20 Hz*

Figure 13 shows the valve inlet and system pressures at a 25% duty cycle. Again, the model captures the pressure rise very well. As seen with 50% duty cycle the simulation experiences a high frequency oscillation not observed in the measured data.

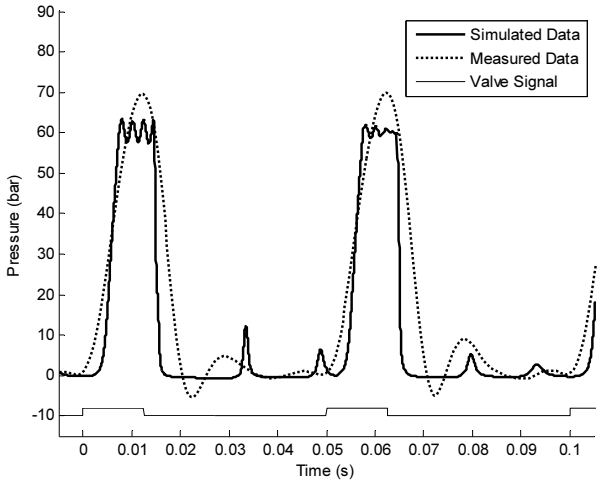

Fig. 13: *Valve Inlet Pressure @ 25 % duty cycle, 20 Hz*

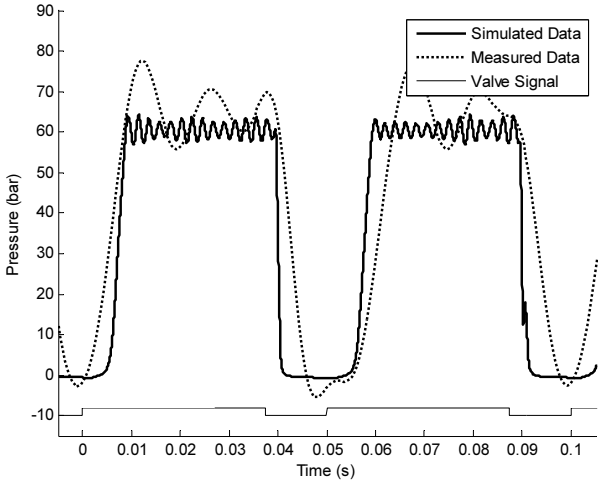

Fig. 14: *Valve Inlet Pressure @ 75 % duty cycle, 20 Hz*

Figure 14 shows the valve inlet pressure at a 75 % duty cycle with the same differences found as noted for Fig. 11 and 13.

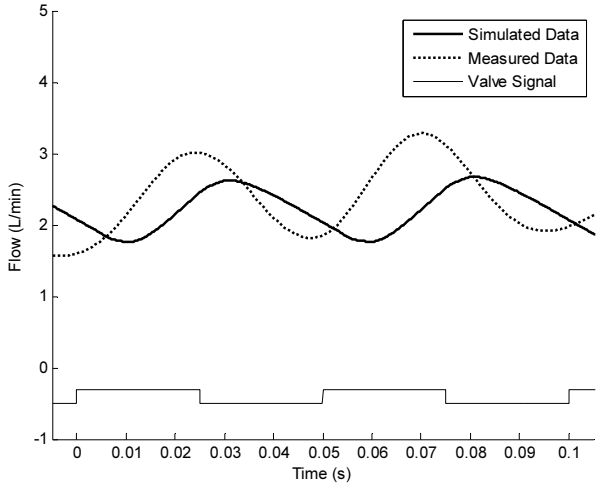

Fig. 15: *System Flow @ 50% duty cycle, 20 Hz*

The plot in Fig. 15 shows a typical flow ripple comparison between the measured and simulated data with generally good agreement between the average flow and frequency (with a small phase shift). The model slightly under predicts flow ripple magnitude.

The efficiencies and system duty cycles for 25 %, 50 %, and 75 % valve duty cycles where determined using the following equations:

$$Eff = \frac{\int_{t=0}^{t=t_{\text{Final}}} p_{\text{system}} q_{\text{system}} dt}{\int_{t=0}^{t=t_{\text{Final}}} p_{\text{inlet}} q_{\text{inlet}} dt} \quad (15)$$

$$\%duty_{\text{system}} = \frac{\int_{t=0}^{t=t_{\text{Final}}} q_{\text{system}} dt}{\int_{t=0}^{t=t_{\text{Final}}} q_{\text{inlet}} dt} \quad (16)$$

These equations were used for the experimental and simulated data. It should be noted again however, that this method of modeling efficiency does not include pump losses, and only considers the efficiency of the metering portion of the system. Table 2 provides a summary of the measured and simulated efficiencies and duty cycles.

Table 2: Comparison of Measured and Simulated Efficiencies and Duty Cycles as a Function of Duty Cycle

Switching Frequency	[Hz]	20	20	20
Cmd Duty Cycle	[%]	25	50	75
Simulated Efficiency	[%]	41.9	49.7	52.1
Measured Efficiency	[%]	31.8	49.5	54.6
Simulated Duty Cycle	[%]	8.3	22.5	35.2
Measured Duty Cycle	[%]	8.3	24.8	38.5

The model adequately captures the efficiency of the system at medium and high duty cycles. At the 25 % duty cycle the accumulator is not able to maintain the flow required by the relief valve and there are periods of no flow. This leads to a measured system efficiency that is significantly lower than predicted.

4.3 Effect of Switching Frequency

While holding the duty cycle fixed at 50 %, the effects of changing the switching frequency were investigated with both simulation and measurement. The valve inlet pressure at a switching frequency of 20 Hz was given in Fig. 11, 40 Hz in Fig. 16, and 60 Hz in Fig. 17. All plots show reasonable agreement between the measured and simulated results.

Figure 16 shows that as driving frequency increases to 40 Hz the valve spends more time in transition. This lowers the effective system flow rate out for a given duty cycle, and decreases efficiency.

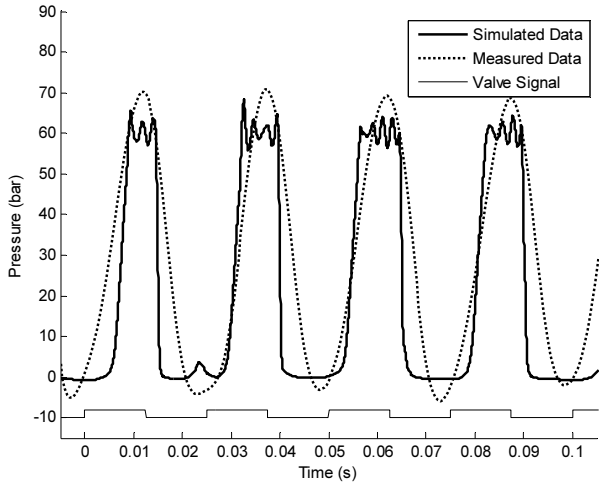

Fig. 16: *Valve Inlet Pressure @ 50 % duty cycle, 40 Hz*

Figure 17 shows that at 60 Hz, the valve is in transisiton the majority of the time. This results in an even lower efficiency as compared with 20 Hz and 40 Hz.

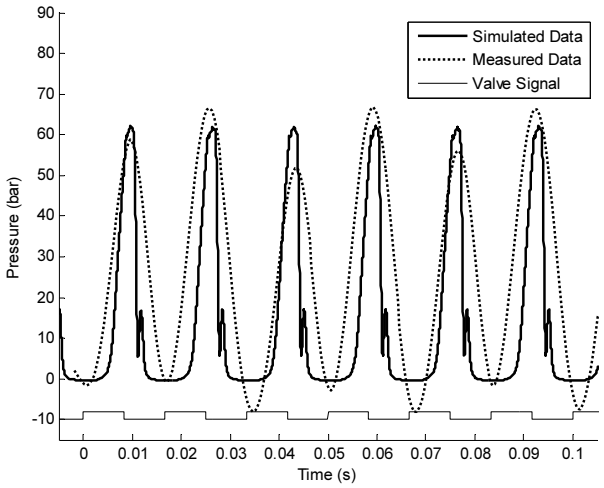

Fig. 17: *Valve Inlet Pressure @ 50 % duty cycle, 60 Hz*

Using Eq. 15 and 16 again for efficiency and duty cycle, the measured and simulated results can be compared relative to varying the switching frequency. These are presented in Table 3.

Table 3: Comparison of Measured and Simulated Efficiencies and Duty Cycles as a Function of Switching Frequency

Switching Frequency [Hz]	20	40	60
Cmd Duty Cycle [%]	50	50	50
Simulated Efficiency [%]	49.7	41.2	22.4
Measured Efficiency [%]	49.5	34.1	17.4
Simulated Duty Cycle [%]	22.5	15.3	5.6
Measured Duty Cycle [%]	24.8	16.5	8.5

As Table 3 illustrates, increasing the switching frequency results in a lower actual duty cycle and efficiency. This was demonstrated in the actual system and the model. This lowest efficiency occurs at 60 Hz because the valve is in transition for a larger portion of each cycle which increases transition losses.

5 Simulated Effects of Line Lengths and Volumes on Efficiency

After completion of the experimental testing, the model was used to simulate the effects of line lengths and volumes on VVDP system efficiency. By decreasing line lengths, the effects of fluid inertia are decreased. By decreasing trapped volumes, the losses associated with fluid compressibility are decreased.

5.1 Reduced Valve Leakage

The experimental testing used a prototype valve that had had relatively low tolerances and therefore significant leakage (measured up to 5 L/min at higher pressures). Fig. 18 illustrates the leakage through the sliding sealing surfaces of the valve when port A is pressurized (when the valve is switched to connect the pump flow to the system).

Since this leakage flow was a function of locally available machining tolerances (70 microns radial clearance) and could be effectively eliminated with standard production valve clearances. It was removed from the remaining simulations to show what efficiencies a reasonably (optimally) configured VVDP might be capable of and to evaluate the effects of changing compressible volumes and line lengths (resistive flow losses).

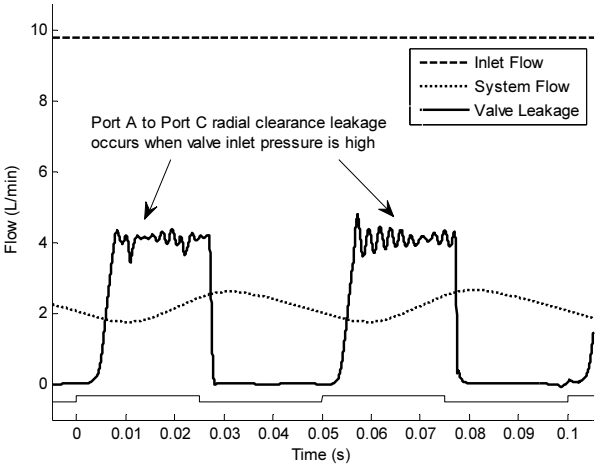

Fig. 18: *Flows and Valve Leakage @ 50% duty cycle, 40 Hz*

5.2 Reduced Compressible Volume

The experimental system had approximately 70 cc of compressible volume. 20 cc are located within the pump, 30 cc are located within the on/off valve, and 20 cc are between the on/off valve and the check-valve. These volumes were determined primarily by the choice of commercially available components and the methods of connecting everything together. In an integrated VVDP system these volumes could be significantly reduced and it is the goal of this section to study the influence of line lengths and volumes on system efficiency.

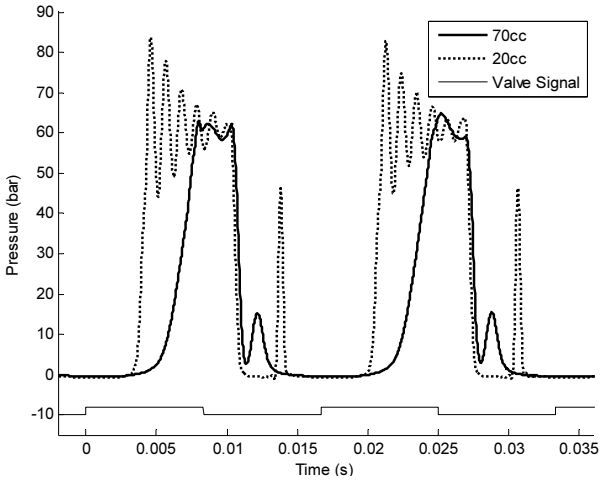

Fig. 19: *Valve Inlet Pressure @ 50 % duty cycle, 60 Hz*

When the compressible volume is reduced the pressure rise and decay rates are faster, resulting in fewer losses (more flow to the system each switch and less discarded energy during decompression).

To determine the effect of compressibility, the compressible volume was reduced to 25 % of the original, or 17.5 cc total. The plot for this simulation at a switching frequency of 60 Hz is shown in Fig. 19.

When compared to the pressure trace of the original system with a 70 cc compressible volume, the pressure rise time was greatly reduced for the 17.5 cc compressible volume system. This resulted in improved efficiency as compared to the 70 cc volume. The comparison of results for 20 Hz, 40 Hz, and 60 Hz is shown in Table 4.

Table 4: Comparison of Simulated Efficiencies and Duty Cycles as a Function of Compressible Volume

Switching Frequency	**[Hz]**	20	40	60
Cmd Duty Cycle	**[%]**	50	50	50
Efficiency w/17.5 cc	**[%]**	90.4	87.1	83.4
Efficiency w/70 cc	**[%]**	87.1	75.9	52.7
Duty Cycle w/17.5 cc	**[%]**	45.5	41.7	36.7
Duty Cycle w/70 cc	**[%]**	39.8	27.9	14.5

Remembering that the internal valve leakage has been removed, it is seen in Table 4 that decreasing the compressible volume resulted in increased system efficiency and effective duty cycle, especially for a system operating at a higher on/off valve switching frequency. Since the compressibility losses occur at each switch they become more critical as switching frequency is increased, therefore the largest improvements in efficiency were seen at 60 Hz relative to 20 Hz.

5.3 Reduced Line Length

The simulated efficiencies calculated in Table 5 resulted from decreasing the line lengths to 25 % of the original (122 mm to 30.5 mm) while keeping the compressible volumes the same (70 cc). This change results in lower line resistance and fluid inertia (even though in practice decreasing the line length also decreases the compressible volume), allowing only the effects of line resistance and inertia on system efficiency to be investigated.

Table 5: Comparison of Simulated Efficiencies and Duty Cycles as a Function of Line Length.

Switching Frequency	**[Hz]**	20	40	60
Cmd Duty Cycle	**[%]**	50	50	50
Efficiency 30 mm	**[%]**	86.8	77.3	63.9
Efficiency 122 mm	**[%]**	87.1	75.9	52.7
Duty Cycle 30 mm	**[%]**	40.6	31.3	21.8
Duty Cycle 122 mm	**[%]**	39.8	27.9	14.5

Comparing Tables 4 and 5 demonstrate that the efficiency of a VVDP system is typically more sensitive to compressible volume than to line resistance and fluid inertia.

5.4 Optimized VVDP System

This section considers what minimum compressible volumes and line lengths, and corresponding efficiencies, might be achievable if the design of VVDP pump and valve were optimized by integrating pump and valve into one small package.

By reducing the compressible volume to the lowest reasonable amount of 6 cc and decreasing the line length to 2.5 mm, the efficiency of an optimized system can be investigated. The results of this analysis at 20 Hz can be seen in Fig. 20, where minimal compressible volume system is compared with the experimental system. The pressure rise and decay rates are very fast relative to original system, leading to minimal compressibility losses.

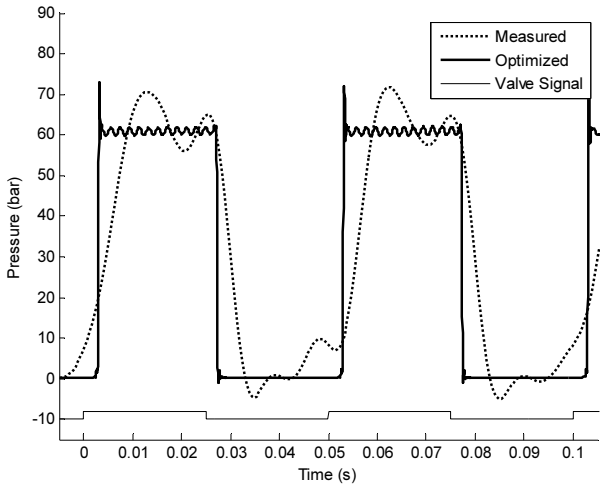

Fig. 20: *Valve Inlet Pressure @ 50 % duty cycle, 20 Hz*

The resulting efficiencies and effective duty cycles for a VVDP system with minimal compressible volume and line lengths are shown in Table 6.

Table 6: Comparison of Simulated Efficiencies and Duty Cycles at Optimal Line Lengths and Volumes

Switching Frequency [Hz]	20	20	20	40	60
Cmd Duty Cycle [%]	25	50	75	50	50
Efficiency 30 mm [%]	90.2	91.6	89.0	89.3	86.8
Efficiency 122 mm [%]	76.0	87.1	86.9	75.9	52.7
Duty Cycle 30 mm [%]	22.4	46.6	68.9	44.1	41.5
Duty Cycle 122 mm [%]	15.6	39.8	61.5	27.9	14.5

As the table shows, significantly higher system efficiency is possible with the optimized system. Across the three switching frequencies the efficiency improved an average of 14 %. Achieving these line lengths and volumes would require careful system design and component integration.

Changing the system pressure will also have an effect on the system efficiency. In general and assuming other parameters remain constant, increasing the system pressure increases the compressibility loss per switch but decreases the effect of the valve metering loss when the valve is directing pump flow to tank. The portion of the valve metering loss when the pump flows to tank remains constant but becomes a smaller portion of the power delivered to the system when the system pressure is increased.

6 Conclusion

The focus of this research was to develop a model of a Virtual Variable Displacement Pump (VVDP) system. The model developed consisted of a pump and prime mover, an on/off valve, a check valve, an accumulator, and line model subsystems. The on/off valve model was based on a detailed coupled lumped parameter model.

The model was validated using a non-optimal experimental setup. This system consisted of a fixed displacement pump driven by an electric motor, 3/2 on/off valve, high speed check valve, accumulator, and load valve. Experimental results were compared to the model.

Once validated, the model was used to determine possible efficiency and noise improvements by removing valve leakage and changing compressible volume and line length. By minimizing the compressible volume and line lengths the maximum efficiency was increased throughout all simulated conditions. These efficiency calculations do not include the pump losses.

Although the study demonstrates that VVDP systems can achieve reasonably high efficiencies relative to low cost systems using a fixed displacement pump and pressure relief valve, careful design integration of the pump and switching valve is important. Compressible volumes, valve dynamics and leakage, and to a lesser extent, line resistance all play an important role in determining the overall performance and efficiency.

Nomenclature

$\%Duty_{system}$	effective duty cycle	[%]
A	line area	[m^2]
A_{cv}	check valve pressurized area	[m^2]
A_{piston}	area of accumulator piston	[m^2]
A_{rel}	relief valve opening area	[m^2]
β	bulk modulus of oil	[Pa]
b_{wall}	wall dampening coefficient	[Ns/m]
d	line diameter	[d]
Eff	system efficiency	[%]
f	line friction factor	[--]
F_{cv_press}	pressure force on check valve	[N]
F_{cv_spring}	spring force on check valve	[N]
F_{cv_wallb}	wall damp. force on ch. valve	[N]
F_{cv_wallk}	wall spring force on ch. valve	[N]
$F_{emag\ A}$	electromagnetic force, coil A	[N]
$F_{emag\ B}$	electromagnetic force, coil B	[N]
$F_{Flow\ B}$	flow force at port B	[N]
$F_{Flow\ C}$	flow force at port C	[N]
$F_{friction\ B}$	friction force at sliding seal A→B	[N]
$F_{friction\ C}$	friction force at sliding seal A→C	[N]
$F_{wall\ b,K}$	damping, spring force at contact	[N]
k_{cv}	check valve spring coefficient	[N/m]
k_{rel}	relief valve pressure coefficient	[m^2/Pa]
k_{wall}	wall sping coefficient	[N/m]
L	line length	[m]
m_{cv}	mass of check valve	[kg]
N	compression constant	[--]
P	fluid density	[kg/m^3]
p_0	accumulator precharge press.	[Pa]
p_A	system pressure at load valve inlet	[Pa]
Δp_{cv}	pressure drop across check valve	[Pa]
p_{iner}	fluid inertia pressure drop	[Pa]
p_{inlet}	valve inlet pressure	[Pa]
p_{line}	line/volume pressure	[Pa]
p_{res}	resistance pressure drop	[Pa]
p_{set}	relief valve cracking pressure	[Pa]
p_{system}	system pressure	[Pa]
p_T	tank pressure	[Pa]
Q_{acc}	accumulator inlet flow	[L/min]
Q_{comp}	compressibiltiy flow	[L/min]
q_{inlet}	valve inlet flow	[L/min]
Q_{line}	line flow	[L/min]
q_{system}	system flow	[L/min]
ΔV	change in accumulator volume	[L]
V_0	intial accumulator volume	[L]
V_{comp}	compressed oil volume	[L]
V_{hold}	hold voltage	[V]
V_{line}	uncompressed line volume	[L]
V_{peak}	peak voltage	[V]
X	accumulator piston postion	[m]
x_{cv}	check valve position	[m]
x_{cv_max}	check valve max position	[m]
x_{cv_wall}	check valve wall protrusion	[m]

Reference

Andruch, J., and **Lumkes, J.** 2008. A Hydraulic System Topography with Integrated Energy Recovery and Reconfigurable Flow Paths Using High Speed Valves, *Proceedings of the 51st National Conference on Fluid Power (NCFP)*, NCFP I08-24.1, pp. 649-657.

Batdorff, M. A. and **Lumkes Jr, J. H.** 2006. Virtually Variable Displacement Hydraulic Pump Including Compressibility and Switching Losses, *Proceedings of IMECE2006*, Chicago, IL, United States.

Grabbel, J. and **Ivantysynova, M.** 2005. An investigation of swash plate control concepts for displacement controlled actuators. *International Journal of Fluid Power*, Vol. 6 (2005), No. 2, pp. 19- 36.

Heybroek, K.; Larsson, J. and **Palmberg, J.O**. 2006. Open Circuit Solution for Pump Controlled Actuators. *Proceedings of 4th FPNI PhD Symposium*, pp. 27-40. Sarasota, Florida, USA.

Li, P., Lie, C. and **Chase, T.** 2005. Software Enabled Variable Displacement Pumps. *Proceedings of IMECE2005*, IMCE2005-81376.

Liu, S. and **Yao, B.** 2002. Energy-saving control of single-rod hydraulic cylinders with programmable valves and improved working mode selection. *SAE Transactions – Journal of Commercial Vehicle*, SAE 2002-01-1343, pp. 51-61.

Mahrenholz, J. 2009. Coupled Multi-Domain Modeling and Simulation of High Speed On/Off Valves: Thesis (MSABE) – Purdue University.

Mahrenholz, J. and **Lumkes, J**. 2009. Analytical Coupled Modeling and Model Validation of Hydraulic On/Off Valves. *J. Dyn. Sys., Meas., Control*, Vol. 131.

Nieling, M., Fronczak, F.J. and **Beachley, N.H.** 2005. Design of Virtually Variable Displacement Pump/Motor. Proceedings of the 50th National Conference on Fluid Power, NCFP 105-10.1.

Shenouda, A. and **Book, W.** 2008. Optimal Mode Switching for a Hydraulic Actuator Controlled with Four-Valve Independent Metering Configuration. *International Journal of Fluid Power*, Vol. 9 (2008), No. 1, pp. 35- 46.

Tu, H. C., Rannow, M. B., Van De Ven, J. D., Wang, M., Li, P. Y. and **Chase, T. R.** 2008. High speed rotary pulse width modulated on/off valve, Proceedings of IMECE2007, Seattle, WA, United States.

Williamson, C., Zimmerman, J. and **Ivantysynova, M.** 2008. Efficiency Study of an Excavator Hydraulic System Based on Displacement-Controlled Actuators. *Bath ASME Symposium on Fluid Power and Motion Control (FPMC 2008)*, pp. 291-307.

John H. Lumkes Jr.
John received the B.S.E. degree from Calvin College in 1990, the M.S.E. from the University of Michigan-Ann Arbor in 1992, and the Ph.D. from the University of Wisconsin-Madison in 1997. From 1997-2004 he was an Assistant and Associate Professor at Milwaukee School of Engineering. In 2004 he joined Purdue University as an Assistant Professor and is active in digital hydraulics, modeling and controls, mechatronics, and advising senior design projects.

Mark A. Batdorff
Mark received the B.S.M.E. degree from Milwaukee School of Engineering in 2004, the M.S.E. from the Purdue University in 2006, and is working towards his Ph.D. in the area of high speed electromagnetics applied to digital hydraulics at Purdue University.

John R. Mahrenholz
John received his undergraduate and Masters degrees in Agricultural and Biological Engineering from Purdue University in 2007 and 2009, respectively. His research interests include dynamic systems analysis, controls, and fluid power systems and component design.